International Journal of Scientific & Engineering Research, Volume 9, Issue 1, January-2018
ISSN 2229-5518

Hint of Predictions of Leptonic δ_{CP} phase from Octant Degeneracy at LBNEs

Gayatri Ghosh
Physics Department, Gauhati University, Assam, India

Abstract—In this work, we discuss how the effect of CP violation discovery potential can be improved at long baseline neutrino experiments (LBNE/DUNE), by combining with its ND (near detector) and reactor experiments. study can be further analysed to resolve entanglement of the quadrant of leptonic CPV phase and Octant of atmospheric mixing angle θ_{23}, at LBNEs. The study is done for both NH (Normal hierarchy) and IH (Inverted hierarchy), HO (Higher Octant) and LO (Lower Octant). We show how leptogenesis can enhance the effect of resolving this entanglement, and how possible values of the leptonic CPV phase can be predicted in this context. Carrying out numerical analysis based on the recent updated experimental results for neutrino mixing angles, we predict the values of the leptonic CPV phase for 152 possible cases. We also confront our predictions of the leptonic CPV phase with the updated global fit and find that five values of δ_{CP} are favoured by BAU constraints. One of the five values matches with the recent global fit value of δ_{CP} (leptonic CPV phase) close to 1.41π in our model independent scenario. A detailed analytic and numerical study of baryogenesis through leptogenesis is performed in this framework in a model independent way..

Index Terms— Baryogenesis, Higher Octant, Lower Octant, Leptogenesis, Leptonic CPV phase, Octant Degeneracy.

———————————— u ————————————

1 INTRODUCTION

With the measurement of reactor angle θ_{13} [1–3] precisely by reactor experiments, the unknown quantities left to be measured in neutrino sector are − leptonic CP violating phase [4–9], octant of atmospheric angle θ_{23} [10–14], mass hierarchy, nature of neutrino etc. Long baseline neutrino experiments (LBNE [15, 16], NOνA [17] , T2K [18], MINOS [19], LBNO [20] etc) may be very promising, in measuring many of these sensitive parameters. Exploring leptonic CP violation (CPV) is one of the most demanding tasks in future neutrino experiments [21]. The relatively large value of the reactor mixing angle θ_{13} measured with a high precision in neutrino experiments [22] has opened up a wide range of possibilities to examine CP violation in the lepton sector. The leptonic CPV phase can be induced by the PMNS neutrino mixing matrix [23] which holds, in addition to the three mixing angles, a Dirac type CP violating phase in general as it exists in the quark sector, and two extra phases if neutrinos are Majorana particles. Even if we do not yet have significant evidence for leptonic CPV, the current global fit to available neutrino data manifests nontrivial values of the Dirac-type CP phase [24, 25]. In this context, possible size of leptonic CP violation detectable through neutrino oscillations can be predicted. Recently, [4], two of us have explored possibiities of improving CP violation discovery potential of newly planned Long-Baseline Neutrino Experiments (earlier LBNE, now called DUNE) in USA. In neutrino oscillation probability expression P($\nu\mu \rightarrow \nu e$) relevant for LBNEs, the term due to significant matter effect, changes sign when oscillation is changed from neutrino to antineutrino mode, or viceversa. Therefore in presence of matter effects, CPV effect is entangled and hence, one has two degenerate solutions - one due to CPV phase and another due to its entangled value. It has been suggested to resolve this issue by combining two experiments with different baselines [26, 27]. But CPV phase measurements depends on value of reactor angle θ_{13}, and hence precise measurement of θ_{13} plays crucial role in its CPV measurements. This fact was utilised recently where we explored different possibilities of improving CPV sensitivity for LBNE, USA. We did so by considering LBNE with

1. Its ND (near detector).
2. And reactor experiments.

We considered both appearance ($\nu\mu \rightarrow \nu e$) and disappearance ($\nu\mu \rightarrow \nu e$) channels in both neutrino and antineutrino modes. Some of the observations made in [4] are

1. CPV discovery potential of LBNE increases significantly when combined with near detector and reactor experiments.
2. CPV violation sensitivity is more in LO (lower octant) of atmospheric angle $\theta 23$, for any assumed true hierarchy.
3. CPV sensitivity increases with mass of FD (far detector).
4. When NH is true hierarchy, adding data from reactors to LBNE improve its CPV sensitivity irrespective of octant.

Aim of this work is to critically analyse the results presented in [4], in context of entanglement of quadrant of CPV phase and octant of θ_{23}, and hence study the role of leptogenesis (and baryogenesis) in resolving this enganglement. Though in [4], we studied effect of both ND and reactor experiments on CPV sensitivity of the LBNEs, in this work we have considered only the effect of ND. But similar studies can also be done for the effect of Reactor experiments on LBNEs as well. The details of LBNE and ND are same as in [4]. Following the results of [4], either of the two octants is favoured, and the enhancement of CPV sensitivity with respect to its quadrant is utilized here to calculate the values of lepton-antilepton symmetry. This is done considering two cases of the rotation matrix for the fermions - CKM only, and CKM+PMNS. Then, this is used to calculate the value of BAU. This is an era of precision measurements in neutrino physics. We therefore consider variation of Δm^2_{31} within its 1σ, 2σ and 3σ range values. We calculate baryon to photon ratio, and compare with its experimentally known best fit value. We observe that the BAU can be explained most favourably for five possible cases explored here: IH, $\delta_{CP} = 1.43\pi$ and HO of $\theta 23$; IH, $\delta_{CP} = 0.5277\pi$ and HO of

θ_{23}; IH, $\delta_{CP} = 0.488\pi$ and LO of θ_{23}; IH, $\delta_{CP} = 0.383\pi$ and HO of θ_{23}; IH, $\delta_{CP} = 1.727\pi$ and LO of θ_{23}. It is worth mentioning that the value of $\delta_{CP} = 1.43\pi$ favoured by our calculation here is close to the central value of δ_{CP} from the recent global fit result [25, 28]. We also find that for variation of $\Delta m2_{31}$, within its 1σ range, the calculated values of ηB for all possible five cases mentioned above lie in the allowed range of its best fit value. But for 3 σ variation of $\Delta m2_{31}$, some of its values at its 3σ C.L are disfavoured. Also for the variation of θ_{13} within its 3 σ C.L, its values around 9.0974 are favoured, as far as matching with the best fit values of η_B are concerned. These results could be important keeping in view that the quadrant of leptonic CPV phase, and octant of atmospheric mixing angle θ_{23} are yet not fixed. Also, they are significant in context of precision measurements on neutrino oscillation parameters. The paper is organized as follows. In Section 2, we discuss entanglement of quadrant of CPV phase and octant of θ_{23}. In Sec. 3 we show how the baryon asymmetry (BAU) within the SO(10) model, by using two distinct forms for the lepton CP asymmetry, can be used to break the entanglement. Sec. 4 summarizes the work.

2 OCTANT OF Θ_{23}

2.1 CP Asymmetry

As discussed above, from Fig. 3 of [4], we find that by combining with ND and reactor experiments, CPV sensitivity of LBNE improves more for LO (lower octant) than HO (higher octant), for any assumed true hierarchy. From Fig. 1 of [29] we plot CP asymmetry,

$$A_{CP} = \{P(\nu_\mu \rightarrow \nu_e) - P(\nu_\mu \rightarrow \nu_e)\} / \{P(\nu_\mu \rightarrow \nu_e) + P(\nu_\mu \rightarrow \nu_e)\} \quad (1)$$

It was shown in [4] that, using near detector (and combining with reactor experiments) at LBNE, the sentivity to measure CPV phase (and hence CP asymmetry) improves more at lower octant of θ_{23}. CP asymmetry also depends on the mass hierarchy. For NH, CP asymmetry is more in LO than in HO. For IH, CP asymmetry is more in LO than in HO. In this work we have used above information to calculate dependance of leptogenesis on octant of θ_{23} and quadrant of CPV phase. From Fig. 1 of [29] we see that

$$A_{CP}(LO) > A_{CP}(HO) \quad (2)$$

2.2 Quadrant of CPV phase

For a given true hierarchy, there are eight degenerate solutions
δ_{CP} (first quadrant) $-$ θ_{23} (lower octant)

δ_{CP} (second quadrant) $-$ θ_{23}(lower octant)
δ_{CP} (third quadrant) $-$ $\theta_2$3(lower octant)
δ_{CP} (fourth quadrant) $-$ θ_{23}(lower octant)
δ_{CP} (first quadrant) $-$ θ_{23}(higher octant)
δ_{CP} (second quadrant) $-$ θ_{23}(higher octant)
δ_{CP} (third quadrant) $-$ θ_{23}(higher octant)
δ_{CP} (fourth quadrant) $-$ θ_{23}(higher octant) (3)

This eight-fold degeneracy can be viewed as

Quadrant of CPV phase $-$ Octant of θ_{23} (4)

entanglement. Out of these eight degenerate solutions, only one should be true solution. To pinpoint one true solution, this entanglement has to be broken. We have shown [4] that sensitivity to discovery potential of CPV at LBNEs in LO is improved more, if data from near detector of LBNEs, or from Reactor experiments is added to data from FD of LBNEs as shown in Fig. 3 of [4]. Therefore 8-fold degeneracy of (3) gets reduced to 4-fold degeneracy, with our proposal [4]. Hence, following this 4-fold degeneracy still remains to be resolved. δ_{CP} (first quadrant) $-$ θ_{23}(LO) δ_{CP} (second quadrant) $-$ θ_{23}(LO) δ_{CP} (third quadrant) $-$ θ_{23}(LO) δ_{C}P (fourth quadrant) $-$ θ_{23}(LO) (5) The possibility of $\theta_{23} > 45^0$, ie HO of θ_{23} is also considered in this work. In this context the degeneracy is δ_{CP} (first quadrant) $-$ θ_{23}(HO) δ_{CP} (second quadrant) $-$ θ_{23}(HO) δ_{CP} (third quadrant) $-$ θ_{23}(HO) δ_{CP} (fourth quadrant) $-$ θ_{23}(HO) (6) In this work, we propose that leptogenesis can be used to break above mentioned 4-fold degeneracy of Eq. (5),(6). It is known that observed baryon asymmetry of the Universe (BAU) can be explained via leptogenesis [29–33]. In leptogenesis, the lepton-antilepton asymmetry can be explained, if there are complex yukawa couplings or complex fermion mass matrices. This in turn arises due to complex leptonic CPV phases, δ_{CP}, in fermion mass matrices. If all other parameters except leptonic δ_{CP} phase in the formula for lepton - antilepton asymmetry are fixed, for example, then observed value of BAU from experimental observation can be used to constrain quadrant of δ_{CP}, and hence 4-fold entanglement of (5),(6) can be broken. An experimental signature of CP violation associated to the dirac phase δ_{CP}, in PMNS matrix [34], can in principle be obtained, by searching for CP asymmetry in ν flavor oscillation. To elucidate this proposal, we consider model independent scenario, in which BAU arises due to leptogenesis, and this lepton-antilepton asymmetry [35] is generated by the out of equilibrium decay of the right handed, heavy majorana neutrinos, which form an integral part of seesaw mechanism for neutrino masses and mixings. Since our proposal is model independent, we consider type I seesaw mechanism, just for simplicity.

3 ANALYSIS AND DISCUSSION OF RESULTS

For our numerical analysis, we take the current experimental data for three neutrino mixing angles as inputs, which are given at $1\sigma - 3\sigma$ C.L, as presented in [2]. Here, we perform numerical analysis and present results both for normal hierarchy, inverted hierarchy, HO, LO from Fig. 2 of [29]. We have explored the CP asymmetry using Eq. (7)-Eq. (12) of [29] and corresponding baryon asymmetry using Eq. (14)-(16) of [29], for 152 different combinations (shown in Table I-XII) of the two hierarchies (NH and IH), two types of octants– LO and HO, w ND, w/o ND (with and without near detector) and δ_{CP} corresponding to maximum χ^2 (for maximum sensitivity from Fig. 2(a), 2(b)) of [29], for which the CP discovery potential of the DUNE is maximum. We also consider non maximal values of δ_{CP} corresponding to $\chi^2 = 4, 9, 16, 25$ from Fig. 2 of [29]. We

examine these different cases in the light of recent ratio of the baryon to photon density bounds, $5.7\times10{-}10 \leq \eta_B \leq 6.7\times10{-}10$ (CMB), and checked for which of the 152 cases, our calculated value of $|\eta_B|$ lies within this range.

TABLE 1
CALCULATED VALUES OF CP ASYMMETRY ǫL AND BARYON TO PHOTON RATIO IN CASE OF LO, FOR R_{1J} ELEMENTS OF R MATRIX CONSISTING OF U_{PMNS} AND V_{CKM} FOR THE VALUES OF CPV PHASE WHEN THE CP DISCOVERY POTENTIAL OF THE LBNE/DUNE IS MAXIMUM AS SHOWN IN FIG. 2 OF [29].

Case	hierarchy, octant	w ND/ OR w/o ND	δ_{CP}	ϵ_l	$\lvert\eta_B\rvert$
1	NH, LO	WND	101	$-.0000177532$	7.39703×10^{-8}
2	NH, LO	WND	280	$-.0000125002$	5.17312×10^{-8}
3	NH, LO	W/oND	108	.0000153489	6.35202×10^{-8}
4	NH, LO	W/oND	282	7.53352×10^{-6}	3.11769×10^{-8}
5	IH, LO	W/ND	83	2.56383×10^{-6}	1.06102×10^{-8}
6	IH, LO	W/ND	276	1.01403×10^{-6}	4.19647×10^{-9}
7	IH, LO	W/oND	88	1.46427×10^{-7}	6.05975×10^{-10}
8	IH, LO	W/oND	275	3.6845×10^{-6}	1.5248×10^{-8}

TABLE 2
SAME AS IN TABLE 1, EXCEPT HERE R MATRIX CONSISTS OF UPMNS ONLY.

Case	hierarchy, Octant	w ND/ OR w/o ND	δ_{CP}	ϵ_l	$\lvert\eta_B\rvert$
1	NH, LO	WND	101	.0000268767	1.11227×10^{-7}
2	NH, LO	WND	280	.0000238272	9.86068×10^{-8}
3	NH, LO	W/oND	108	.0000231986	9.60055×10^{-8}
4	NH, LO	W/oND	282	.0000332106	1.3744×10^{-7}
5	IH, LO	WND	83	.0000109298	4.5232×10^{-8}
6	IH, LO	W/ND	276	-3.3319×10^{-6}	1.37888×10^{-8}
7	IH, LO	W/oND	88	2.96234×10^{-7}	1.22594×10^{-9}
8	IH, LO	W/oND	270	-9.18963×10^{-7}	3.80305×10^{-9}

We find that out of 32 different cases corresponding to maximal sensitivity χ^2 (from Fig. 2) as shown in Table 1–4, our calculated value of BAU is larger than the currently allowed range of BAU except for two cases: case 7 in table 1 and case 5 in table 3 for which the calculated $|\eta B|$ is compatible with the present range of baryon to photon density ratio [36]. In Table 1, case 7 which has $\delta_{CP} = 88^0$ or 0.488π (first quadrant), IH and atmospheric angle θ_{23} in LO has $\eta_B = 6.05975 \times 10^{-10}$, consistent with its best fit value, $\eta_B = 6.05 \times 10{-}10$ [36]. For this case, $\varrho l = 1.46427 \times 10^{-7}$ lies within the Davidson and Ibbara bounds [37], ($\epsilon_l \leq 4.59 \times 10^{-5}$). In Table III, case 5 has $\delta CP = 950$ or 0.5277π (second quadrant), IH and atmospheric angle θ_{23} in HO has BAU equal to 6.2157×10^{-10} which is in accord with the present $|\eta_B|$ bounds and it leads to CP asymmetry $|\epsilon_l| = 1.50195 \times 10^{-7}$ that lies within the Davidson and Ibarra bounds.

Figure 1 shows the allowed regions of $|\eta_B|$ in the plane charted by (Δm^2_{31}, $|\eta_B|$) for δ_{CP} allowed at maximal sensitivity of CP discovery potential from Fig. 2 of [29] (case 7 of Table 1). Here we show the variation of $|\eta_B|$ with Δm^2_{31}, taking the

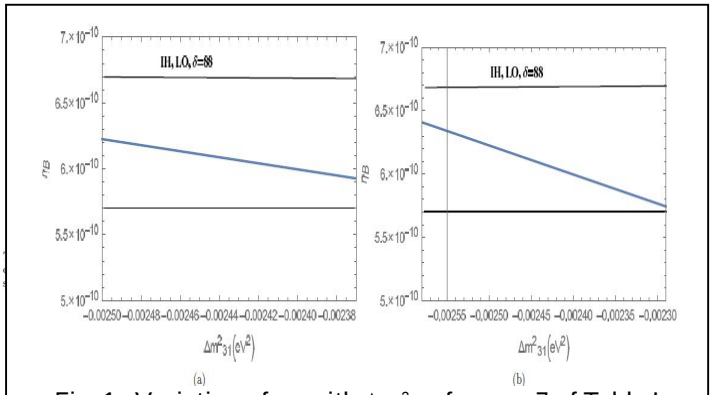

Fig. 1 Variation of η_B with Δm^2_{31}, for case 7 of Table I based on 1σ and 2σ range of Δm^2_{31} in Fig. 3(a) and 3(b) respectively. Plot of η_B Vs Δm^2_{31}[eV ^{2}] with CP phases $\delta_{CP} = 0.488\pi$ for the case when R matrix consists of both VCKM and UPMNS. The blue solid line in Fig. 3(a), 3(b) corresponds to θ23 in LO, δCP = 0.488π (first quadrant) and IH. The black horizontal line corresponds to the upper and lower limit on ηB, 5.7 × 10−10 < ηB < 6.7 × 10−10. As can be seen from the figure, the plots in Fig. 1(a), 1(b) satisfy the current experimental constraints on η_B.

Next, we explore values of δ_{CP} corresponding to $\chi^2 = 4, 9, 16, 25$ from Fig. 2 of ref. [29] for which the CP discovery potential of the LBNE/DUNE is non maximal. For $\chi^2 = 2\,\sigma, 3\sigma$ sensitivity of the CP discovery potential, Table 5-8 summarise the results where we find that out of the 64 possible cases in all, for 63 cases the calculated BAU is larger than the currently allowed range of BAU [36] by almost two to three orders of magnitude except for case 4 of Table VII where $\delta_{CP} = 1.924\,\pi$, IH, HO, has BAU of the order of 8.65034×10^{-12} less than the allowed $|\eta_B|$ limit.

We examine 56 possible cases for non maximal CP discovery sensitivity potential of the LBNE/DUNE from Fig. 2 summarised in Table 9-12 corresponding to $\chi2$ at 4σ, 5σ C.L out of which only 3 cases are consistent with the experimental results of $|\eta B|$ bounds, (a) Case 15 of Table 11 where $\delta_{CP}/\,\pi = 1.43$, ν mass spectrum of IH nature, atmospheric angle θ23 in HO, has CP asymmetry $= 1.48671\times10^{-7}$ which lies within $|\epsilon_l| = 4.59\times10^{-5}$ (Davidson Ibbara bounds) and $|\eta_B| = 6.15262\times10^{-10}$ that agrees with the present BAU range. It is worth noting that this value of $\delta_{CP}/\pi = 1.43$ is close to the central value of δ_{CP} from the recent global fit result [28], (b) Case 13 of Table 11 that locates $\delta_{CP}/\,\pi = 0.3833$, ν mass spectrum of IH nature, θ_{23} in HO, $\epsilon_l = 1.40342 \times 10^{-7}$ ($\leq |\epsilon_l| = 4.59 \times 10^{-5}$) has $|\eta_B| = 5.80973\times 10^{-10}$, consistent with the allowed BAU range. Here R_{1j} elements of R matrix consists of UPMNS and V_{CKM} in both the cases above, (c) Case 4 of Table 12 which has $\delta_{CP}/\pi = 1.727$, IH ν mass spectrum, θ_{23} in LO, $|\epsilon_l| = 1.47958 \times 10^{-7}$ lies within $|\epsilon_l| = 4.59 \times 10^{-5}$ and $|\eta_B| = 6.12311 \times 10^{-10}$

that agrees with the current experimental constraints [36].

TABLE 3
SAME AS IN TABLE 1, BUT HO VALUES ARE USED.

Case	hierarchy, octant	w ND/ w/o ND	δ_{CP}	ϵ_l	$\lvert\eta_B\rvert$
1	NH, HO	*WND*	101	$-.0000189857$	7.85709×10^{-8}
2	NH, HO	*WND*	281	-3.51289×10^{-5}	1.45378×10^{-7}
3	NH, HO	*W/oND*	102	2.72017×10^{-5}	1.12572×10^{-7}
4	NH, HO	*W/oND*	283	-1.82461×10^{-5}	7.551×10^{-8}
5	IH, HO	*W/ND*	95	-1.50195×10^{-7}	6.2157×10^{-10}
6	IH, HO	*W/oND*	94	-8.7785×10^{-8}	3.63291×10^{-10}
7	IH, HO	*W/ND*	281	-5.8547×10^{-6}	2.42292×10^{-8}
8	IH, HO	*W/oND*	272	9.97129×10^{-6}	4.12654×10^{-8}

TABLE 4
SAME AS IN TABLE 3, BUT R MATRIX CONSISTS OF U_{PMNS} ONLY.

Case	hierarchy, octant	w ND/ w/o ND	δ_{CP}	ϵ_l	$\lvert\eta_B\rvert$
1	NH, HO	*WND*	101	.0000268767	1.11227×10^{-7}
2	NH, HO	*WND*	281	.0000112743	4.66576×10^{-8}
3	NH, HO	*W/oND*	102	6.73637×10^{-6}	2.78779×10^{-8}
4	NH, HO	*W/oND*	283	.0000163668	6.77325×10^{-8}
5	IH, HO	*W/ND*	95	4.1771×10^{-6}	1.72891×10^{-8}
6	IH, HO	*W/oND*	94	-1.99098×10^{-6}	8.23952×10^{-9}
7	IH, HO	*W/ND*	281	7.65022×10^{-6}	3.16598×10^{-8}
8	IH, HO	*W/oND*	272	$-.00001093$	4.52369×10^{-8}

Plugging the experimental data for Δm^2_{31} at 3σ C.L, and other ν oscillation parameters at best fit into Eq. (8 - 12) of ref. [29], we predict the values of η_B from Eq. (14, 15, 16) of ref. [29] as shown in the Fig. 2. The figure displays the allowed regions of $|\eta_B|$ in the plane (Δm^2_{13},$|\eta_B|$) for experimental results of Δm^2_{31} at 3σ C.L. In Fig. 2(a) red solid line conforms to the case 15 of Table 11, where $\delta_{CP} = 1.43\pi$, ν mass spectrum of IH structure, atmospherc angle θ_{23} in HO and $|\eta_B|$ in the range consistent with $5.7\times10^{-10} < \eta_B < 6.7\times10^{-10}$ except for $\Delta m^2_{31} > -2.2695\times10^{-3}$eV^2 and $\Delta m^2_{31} < -2.635 \times 10^{-3}$eV^2 where the red solid line departs from the experimental bound on η_B. The orange solid line in Fig. 2(a) depicts case 13 of Table XI which has $\delta_{CP} = 0.383\pi$, ν mass structure of IH spectrum, θ_{23} in HO and $|\eta_B|$ in the allowed range followed by the experimental constraints on $|\eta_B|$ except for $\Delta m^2_{31} > -2.385\times10^{-3}$eV^2. Slight variation of η_B for $\delta_{CP} = 0.5277\pi$ can be seen from Fig. 2(a) for $\Delta m^2_{31} < -2.63 \times 10^{-3}$eV^2 (green solid line). Similarly the green solid line in Fig. 2(b) corresponds to $\delta_{CP} = 0.488\pi$, IH ν spectrum, which is consistent with the allowed range of BAU for $\Delta m^2_{31} < -2.27\times10^{-3}$eV^2. The red solid line in Fig. 4(b) characterises case 4 of Table 12, which has $\delta_{CP} = 1.727\pi$, ν mass structure of IH nature, atmospherc angle θ_{23} in LO and $|\eta_B|$ in the range favoured by the present experimental limit on $|\eta_B|$, $5.7 \times 10^{-10} < |\eta_B| < 6.7 \times 10^{-10}$ except for $\Delta m^2_{31} > -2.255 \times 10^{-3}$eV^2 where the curve fails to fall in the allowed $|\eta_B|$ bounds even at 2σ C.L of Δm^2_{31}.

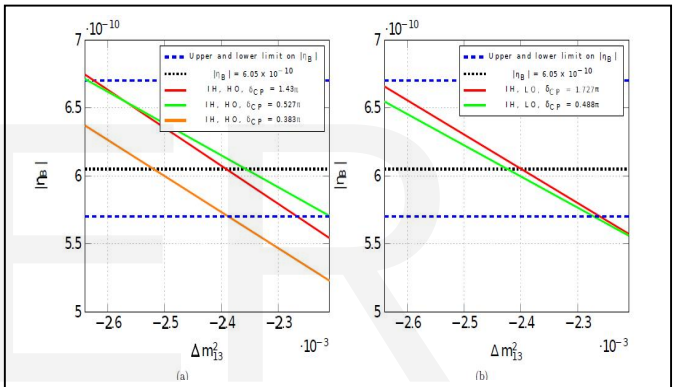

Fig. 2. Variation of η_B with Δm^2_{31} within its 3σ C.L. The upper and lower limit on η_B, $5.7 \times 10^{-10} < \eta_B < 6.7 \times 10^{-10}$ are characterised by blue dashed horizontal lines. Black dotted line corresponds to best fit value, $\eta_B = 6.05 \times 10{-}10$. In the left panel, Fig. 2(a) shows the plot of η_B Vs Δm^2_{31} for $\delta_{CP} = 1.43\pi$, 0.527π,0.383π. Fig. 2(b) of right panel frames the variation of η_B with Δm^2 31 for $\delta CP = 0.488\pi$, 1.727π.

From the above discussion, we conclude that, out of total 152 cases presented in Table 1-12, only for five cases, the values of η_B lie within the experimental limits, which are summarised in Table 13.

Figure 3 completes our discussion by showing the allowed regions in the plane (θ_{13},$|\eta_B|$) which is done for five cases favoured by our analysis above. The shapes of the curves are somewhat symmetrical in Fig. 3(c) and 3(d) about $\theta_{13} = 90$ for $\delta_{CP} = 1.43\pi$, IH, θ_{23} in HO and $\delta_{CP} = 0.383\pi$, IH, θ_{23} in HO. For, $\delta_{CP} = 257.5^0$, values of θ_{13} around 9.0974^0 to 9.1^0, $9.2^0$to 9.22^0, 8.94^0 to 8.97^0, 8.82^0 to 8.84^0 are favoured which agrees well with the global fit value of θ_{13} [28]. For, $\delta_{CP} = 69^0$, values of θ_{13} around 9.0874^0 to 9.1^0, $9.21^0$to 9.2^0, 8.945^0 to 8.99^0 , 8.85^0 are favoured for $5.7\times10^{-10} < \eta_B < 6.7\times10^{-10}$ which is compatible with the global fit value of θ_{13} [28]. For, $\delta_{CP} = 88^0$ in Fig. 3(a), IH, θ_{23} in LO, values of θ_{13} around 9.0974^0 to 9.103^0, $9.61^0$to

9.65^0 are favoured for $5.7 \times 10^{-10} < \eta_B < 6.7\times 10^{-10}$. Similarly for, $\delta_{CP} = 311^0$ in Fig. 3(e), IH, θ_{23} in LO, values of θ_{13} around 9.0974^0 to 9.12^0, 9.72^0 to 9.78^0 are mostly favoured for $5.7\times10^{-10} < \eta_B < 6.7\times10^{-10}$ which is consistent with the global fit data of θ_{13} at 2σ and 3σ C.L [28]. Lastly for $\delta_{CP} = 95^0$ in Fig. 3(b), IH, θ_{23}

TABLE 5

CALCULATED VALUES OF CP ASYMMETRY QF AND BARYON TO PHOTON RATIO IN CASE OF NH, FOR R_{1J} ELEMENTS OF R MATRIX CONSISTING OF U_{PMNS} AND V_{CKM} FOR DUNE/LBNE WITH ITS NEAR DETECTOR, WITH $X^2 = 4$ AND 9 MEASURING CP DISCOVERY SENSITIVITY FROM FIG. 2. OF [29].

Case	hierarchy, Octant	$\Delta\chi^2$	δ_{CP}	ϵ_l	$\lvert\eta_B\rvert$
1	NH, LO	4	17	-3.57328×10^{-5}	1.4787×10^{-7}
2	NH, LO	9	38	1.91122×10^{-5}	7.90943×10^{-8}
3	NH, LO	9	147	3.19392×10^{-5}	1.32178×10^{-7}
4	NH, LO	4	154	3.33001×10^{-6}	1.3781×10^{-8}
5	NH, LO	4	203.5	3.31724×10^{-5}	1.37281×10^{-7}
6	NH, LO	9	213	1.18422×10^{-5}	4.9008×10^{-8}
7	NH, LO	9	332	-7.01565×10^{-6}	2.90337×10^{-8}
8	NH, LO	4	346.5	1.72854×10^{-6}	7.15341×10^{-9}
9	NH, HO	4	17	-3.6128×10^{-5}	1.49513×10^{-7}
10	NH, HO	4	155	-2.65416×10^{-5}	1.0984×10^{-7}
11	NH, HO	4	203	3.76207×10^{-5}	1.5569×10^{-7}
12	NH, HO	4	347.5	8.3309×10^{-7}	3.44768×10^{-9}
13	NH, HO	9	38.3	-1.54969×10^{-5}	6.41328×10^{-8}
14	NH, HO	9	147	3.09483×10^{-5}	1.28077×10^{-7}
15	NH, HO	9	212	-3.30145×10^{-5}	1.36628×10^{-7}
16	NH, HO	9	333.5	-1.97211×10^{-6}	8.16144×10^{-9}

in HO, values of θ_{13} around 9.0974^0 to 9.11^0, 9.52^0 to 9.54^0 are mostly favoured for $5.7 \times 10^{-10} < \eta_B < 6.7 \times 10^{-10}$ compatible with global fitting of θ_{13} at 2σ and 3σ C.L [28].

Our calculated values of Jarkslog invariant by plugging input for the three ν mixing angles at its best fit for favoured cases of BAU and the values of leptonic δ_{CP} phase are summarised in Table 13. We find that for all the five favoured cases, our calculated values of J_{CP} lie within its present experimental limits. In Fig. 4 we plot J_{CP} Vs θ_{13}, taking variation of θ_{13} within 3σ range of its best fit value and find that the plot for all the above listed five cases, J_{CP} lies within its present experimental limits.

TABLE 6

SAME AS IN TABLE 5, BUT R = U_{PMNS} ONLY.

Case	hierarchy, Octant	$\Delta\chi^2$	δ_{CP}	ϵ_l	$\lvert\eta_B\rvert$
1	NH, LO	4	17	1.76335×10^{-5}	7.2975×10^{-8}
2	NH, LO	9	38	1.88675×10^{-5}	7.80817×10^{-8}
3	NH, LO	9	147	-3.2199×10^{-5}	1.33253×10^{-7}
4	NH, LO	4	203.5	-3.28826×10^{-6}	1.36082×10^{-7}
5	NH, LO	4	154	4.1195×10^{-6}	1.70482×10^{-8}
6	NH, LO	9	213	-3.16969×10^{-5}	1.31175×10^{-7}
7	NH, LO	9	332	-3.00567×10^{-5}	1.24385×10^{-7}
8	NH, LO	4	346.5	3.20414×10^{-5}	1.32601×10^{-7}
9	NH, HO	4	17	1.76335×10^{-5}	7.2975×10^{-8}
10	NH, HO	4	155	2.83588×10^{-5}	1.1736×10^{-7}
11	NH, HO	4	203	3.10849×10^{-5}	1.28642×10^{-7}
12	NH, HO	4	347.5	-2.16746×10^{-5}	8.96988×10^{-8}
13	NH, HO	9	38.3	3.10849×10^{-5}	1.28642×10^{-7}
14	NH, HO	9	147	-3.2199×10^{-5}	1.33253×10^{-7}
15	NH, HO	9	212	3.82461×10^{-6}	1.58278×10^{-8}
16	NH, HO	9	333.5	2.77229×10^{-7}	1.14729×10^{-7}

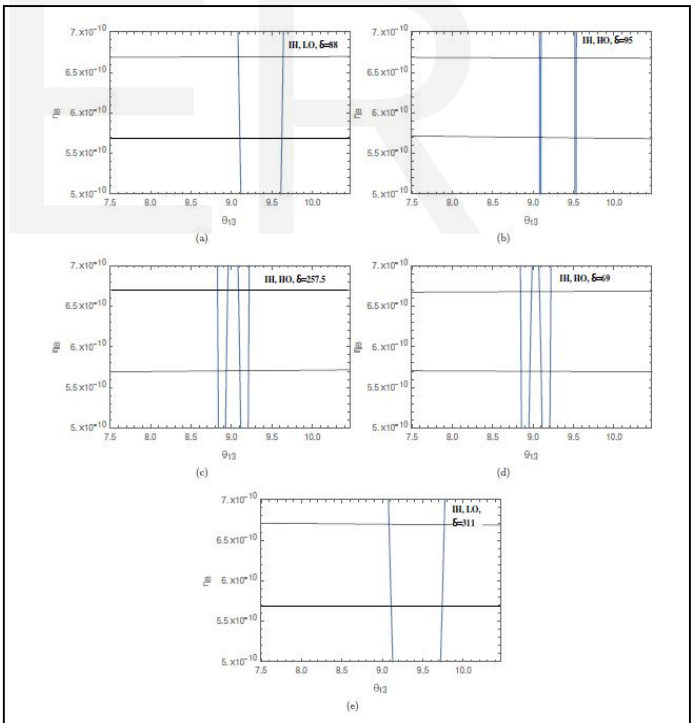

Fig. 3. Plot of η_B vrs θ_{13} with CP phases in Fig. 3(a) $\delta_{CP} = 88^0$, IH, LO; in Fig. 3(b) $\delta_{CP} = 95^0$, IH, HO; in Fig. 5(c) $\delta_{CP} = 257.5^0$, IH, HO; in Fig. 3(d) $\delta_{CP} = 69^0$, IH, HO and in Fig. 3(e) $\delta_{CP} = 311^0$, IH, LO within the 3 σ errors of the best fit values of θ_{13} for the favoured cases. The black solid horizontal line corresponds to the upper and lower limit on η_B, $5.7 \times 10^{-10} < \eta_B < 6.7 \times 10^{-10}$.

TABLE 7
SAME AS IN TABLE 5, BUT IH IS USED.

Case	hierarchy, Octant	$\Delta\chi^2$	δ_{CP}	ϵ_l	$\lvert\eta_B\rvert$
1	IH, HO	4	13.5	4.91465×10^{-6}	2.03389×10^{-8}
2	IH, HO	4	157.5	-7.63368×10^{-7}	3.15914×10^{-9}
3	IH, HO	4	202	1.24531×10^{-6}	5.15362×10^{-9}
4	IH, HO	4	346.3	-2.09025×10^{-9}	8.65034×10^{-12}
5	IH, HO	9	29	-5.98012×10^{-6}	2.47483×10^{-8}
6	IH, HO	9	153	1.18773×10^{-5}	4.91533×10^{-8}
7	IH, HO	9	209	8.38787×10^{-6}	3.47125×10^{-8}
8	IH, HO	9	332.5	2.45147×10^{-7}	1.01449×10^{-9}
9	IH, LO	9	332.5	1.03435×10^{-6}	4.28058×10^{-9}
10	IH, LO	9	209	5.36981×10^{-6}	2.22225×10^{-8}
11	IH, LO	9	153	7.94367×10^{-6}	3.28743×10^{-8}
12	IH, LO	9	29	-7.28224×10^{-6}	3.0137×10^{-8}
13	IH, LO	4	346.1	-1.04874×10^{-6}	4.34013×10^{-9}
14	IH, LO	4	203	1.26601×10^{-5}	5.23928×10^{-8}
15	IH, LO	4	157.5	-9.9942×10^{-7}	4.13602×10^{-9}
16	IH, LO	4	13.5	-3.75736×10^{-7}	1.55496×10^{-9}

TABLE 8
SAME AS IN TABLE VI, BUT IH IS USED.

Case	hierarchy, Octant	$\Delta\chi^2$	δ_{CP}	ϵ_l	$\lvert\eta_B\rvert$
1	IH, HO	4	13.5	4.00427×10^{-6}	1.65714×10^{-8}
2	IH, HO	4	157.5	3.11981×10^{-6}	1.29111×10^{-8}
3	IH, HO	4	202	3.99325×10^{-6}	1.65258×10^{-8}
4	IH, HO	4	346.3	4.15622×10^{-6}	1.72002×10^{-8}
5	IH, HO	9	29	4.15708×10^{-6}	1.72038×10^{-8}
6	IH, HO	9	153	-3.99333×10^{-6}	1.65267×10^{-8}
7	IH, HO	9	209	-7.0083×10^{-7}	2.90033×10^{-9}
8	IH, HO	9	332.5	-3.56253×10^{-6}	1.47433×10^{-8}
9	IH, LO	9	332.5	1.03435×10^{-6}	4.28058×10^{-9}
10	IH, LO	9	209	-7.0083×10^{-7}	2.90033×10^{-9}
11	IH, LO	9	153	-3.99333×10^{-6}	1.65261×10^{-8}
12	IH, LO	9	29	4.15708×10^{-6}	1.72038×10^{-8}
13	IH, LO	4	346.1	3.63103×10^{-6}	1.50267×10^{-8}
14	IH, LO	4	203	-2.80629×10^{-6}	1.16136×10^{-8}
15	IH, LO	4	157.5	3.11981×10^{-6}	1.29111×10^{-8}
16	IH, LO	4	13.5	4.000427×10^{-6}	1.65714×10^{-8}

TABLE 9
SAME AS IN TABLE V, BUT FOR X^2 = 16 AND 25

Case	hierarchy, Octant	$\Delta\chi^2$	δ_{CP}	ϵ_l	$\lvert\eta_B\rvert$
1	NH, LO	16	56	1.35794×10^{-5}	5.62719×10^{-8}
2	NH, LO	16	136	-3.11475×10^{-5}	1.28902×10^{-7}
3	NH, LO	16	232	1.37456×10^{-5}	5.68851×10^{-8}
4	NH, LO	16	314	1.49244×10^{-6}	6.17636×10^{-9}
5	NH, LO	25	84	3.56574×10^{-5}	1.47565×10^{-7}
6	NH, LO	25	122.5	7.31569×10^{-6}	3.02754×10^{-8}
7	NH, LO	25	263.5	-1.25402×10^{-5}	5.18967×10^{-8}
8	NH, LO	25	294.5	4.28344×10^{-6}	1.77267×10^{-8}
9	NH, HO	16	59	3.19255×10^{-5}	1.32121×10^{-7}
10	NH, HO	16	132.5	-1.70443×10^{-5}	7.05367×10^{-8}
11	NH, HO	16	232.25	8.92875×10^{-6}	3.69509×10^{-8}
12	NH, HO	16	314	4.8229×10^{-6}	1.99592×10^{-8}

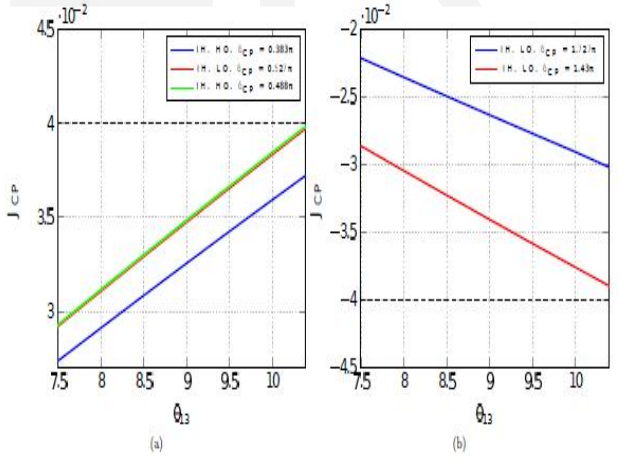

Fig. 4. Plot of J_{CP} vrs θ_{13} with CP phases in Fig. 6(a):$\delta_{CP} = 95^0$, IH, HO; $\delta_{CP} = 69^0$, IH, HO; $\delta_{CP} = 88^0$, IH, LO. Fig. 6(b): $\delta_{CP} = 257.5^0$, IH, HO; $\delta_{CP} = 311^0$, IH, LO within the 3 σ C.L of the best fit values of θ_{13}. Horizontal line represents the maximum allowed CP violation in the leptonic sector, $J_{CP} \leq .04|\text{Sin}\delta_{CP}|$.

TABLE 10
SAME AS IN TABLE VI, BUT FOR $X^2 = 16$ AND 25

Case	hierarchy, Octant	$\Delta\chi^2$	δ_{CP}	ϵ_l	$\lvert\eta_B\rvert$
1	NH, LO	16	56	-2.96623×10^{-5}	1.2275×10^{-7}
2	NH, LO	16	136	3.22739×10^{-5}	1.33563×10^{-7}
3	NH, LO	16	232	-2.72203×10^{-5}	1.12649×10^{-7}
4	NH, LO	16	314	-1.04375×10^{-5}	4.31949×10^{-8}
5	NH, LO	25	84	-3.32343×10^{-5}	1.37537×10^{-7}
6	NH, LO	25	122.5	-1.47354×10^{-6}	6.09812×10^{-9}
7	NH, LO	25	263.5	-2.36179×10^{-5}	9.77404×10^{-8}
8	NH, LO	25	294.5	-3.32892×10^{-6}	1.37765×10^{-7}
9	NH, HO	16	59	-3.27271×10^{-5}	1.35438×10^{-7}
10	NH, HO	16	132.5	-2.97961×10^{-5}	1.23309×10^{-7}
11	NH, HO	16	232.25	-1.46679×10^{-5}	6.07021×10^{-8}
12	NH, HO	16	314	-1.04375×10^{-5}	4.31949×10^{-8}

TABLE 11
SAME AS IN TABLE 9, BUT IH IS USED.

Case	hierarchy, Octant	$\Delta\chi^2$	δ_{CP}	ϵ_l	$\lvert\eta_B\rvert$
1	IH, LO	25	59	7.35254×10^{-6}	3.04279×10^{-8}
2	IH, LO	25	131.5	1.00443×10^{-6}	4.15675×10^{-9}
3	IH, LO	25	246.5	3.71415×10^{-6}	1.53707×10^{-8}
4	IH, LO	25	311	3.74283×10^{-7}	1.54894×10^{-9}
5	IH, LO	16	42	-7.26506×10^{-6}	3.00659×10^{-8}
6	IH, LO	16	140.5	7.91014×10^{-6}	3.27355×10^{-8}
7	IH, LO	16	225.5	8.74966×10^{-7}	3.62098×10^{-9}
8	IH, LO	16	320.5	8.74965×10^{-7}	3.62097×10^{-9}
9	IH, HO	16	45	-1.88492×10^{-6}	7.80058×10^{-9}
10	IH, HO	16	139	-2.36693×10^{-7}	9.79536×10^{-10}
11	IH, HO	16	226.5	-7.81644×10^{-7}	3.23477×10^{-9}
12	IH, HO	16	319	-3.88288×10^{-6}	1.6069×10^{-8}
13	IH, HO	25	72	1.40342×10^{-7}	5.80793×10^{-10}
14	IH, HO	25	123	-3.73584×10^{-6}	1.54604×10^{-8}
15	IH, HO	25	257.5	1.48671×10^{-7}	6.15262×10^{-10}
16	IH, HO	25	302	-7.71976×10^{-7}	3.19476×10^{-9}

4 CONCLUSION

To break the quadrant of CPV phase − Octant of θ_{23} entanglement we have calculated BAU (η_B) for 152 cases as shown in Tables 1-12, and found that only for five cases, our calculated η_B lies within the present best fit values of η_B. These five cases are $\delta_{CP} = 1.43\pi$ (third quadrant), $\delta_{CP} = 0.527\pi$ (second quadrant), $\delta_{CP} = .383\pi$ (first quadrant), $\delta_{CP} = .488\pi$ (first quadrant) for the case when R matrix consists of both V_{CKM} and U_{PMNS} and $\delta_{CP} = 1.727\pi$ (fourth quadrant), for the case when R matrix consists of U_{PMNS} only. Next, we studied variation of η_B, w.r.t 1σ, 2σ and 3σ variation of Δm^2_{31}, as shown in Figs. 1 and 2. It can be seen from Fig. 1 and 2 that for variation of Δm^2_{31}, within its 1σ range, all calculated values of η_B lie in the allowed range of its best value. For Δm^2_{31} at its 3 σ C.L, the case $\delta_{CP} = 0.488\pi$ is consistent with the allowed range of BAU for $\Delta m^2_{31} < -2.27 \times 10^{-3}\text{eV}^2$. Similarly, very slight discrepancy of ηB for $\delta_{CP} = 0.5277\pi$ can be seen from Fig. 2(a) for $\Delta m^2_{31} < -2.63 \times 10^{-3}\text{eV}^2$. Case 15 of Table 11, where $\delta_{CP} = 1.43\pi$ has $|\eta_B|$ in the range compatible with $5.7 \times 10{-}10 < \eta_B < 6.7 \times 10{-}10$ except for $\Delta m^2_{31} > -2.2695 \times 10^{-3}\text{eV}^2$ and $\Delta m^2_{31} < -2.635 \times 10^{-3}\text{eV}^2$. It is worth noting that this value of $\delta_{CP}/\pi = 1.43$ is close to the central value of δ_{CP} from the recent global fit result [28]. Case 13 of Table 11: $\delta_{CP} = 0.383\pi$ has $|\eta_B|$ in the range allowed by, $5.7 \times 10^{-10} < \eta_B < 6.7 \times 10^{-10}$ except for $\Delta m^2_{31} > -2.385 \times 10^{-3}\text{eV}^2$. Case 4 of Table 12, where $\delta_{CP} = 1.727\pi$, has $|\eta_B|$ in the range favoured by the present experimental constraints except for $\Delta m^2_{31} > -2.255 \times 10{-}^3\text{eV}^2$ where the straight line fails to satisfy allowed $|\eta B|$ bounds even at 2σ C.L of Δm^2_{31}. Interestingly here leptonic CPV phase $\delta_{CP} = 1.727\pi$ lies within the 1σ ranges of δ_{CP} from latest global fit analysis, $\delta_{CP} = 1.67{+}0.37\ {-}0.77$ [28]. Here R_{1j} elements of R matrix consists of only UPMNS elements.

In fig. 3 we showed variations of η_B with θ_{13}, taking range of θ_{13} within 3σ values of its best fit values, for the five favoured cases and find that values of θ_{13} around 9.0974^0 to 9.12^0 (which agrees well with the current fit data [28]) are favoured as far as matching with the best fit values of $|\eta_B|$ are concerned.

TABLE 12

SAME AS IN TABLE 10 BUT IH IS USED.

Case	hierarchy, Octant	$\Delta\chi^2$	δ_{CP}	ϵ_I	$\lvert\eta_B\rvert$
1	IH, LO	25	59	-4.11136×10^{-6}	1.70145×10^{-8}
2	IH, LO	25	131.5	-3.26348×10^{-6}	1.35057×10^{-8}
3	IH, LO	25	246.5	9.54714×10^{-7}	3.95101×10^{-9}
4	IH, LO	25	311	1.47958×10^{-7}	6.12311×10^{-10}
5	IH, LO	16	42	3.06981×10^{-6}	1.27042×10^{-8}
6	IH, LO	16	140.5	4.12475×10^{-6}	1.707×10^{-8}
7	IH, LO	16	225.5	4.11818×10^{-6}	1.70428×10^{-8}
8	IH, LO	16	320.5	-4.80846×10^{-7}	1.98994×10^{-9}
9	IH, HO	16	45	3.74039×10^{-6}	1.54905×10^{-8}
10	IH, HO	16	139	4.18492×10^{-7}	1.73189×10^{-8}
11	IH, HO	16	226.5	2.40081×10^{-6}	9.93556×10^{-9}
12	IH, HO	16	319	-1.06298×10^{-6}	4.39907×10^{-9}
13	IH, HO	25	72	-9.54837×10^{-7}	3.95152×10^{-9}
14	IH, HO	25	123	3.41971×10^{-6}	1.91552×10^{-8}
15	IH, HO	25	257.5	1.81927×10^{-6}	7.52892×10^{-9}
16	IH, HO	25	302	3.04466×10^{-6}	1.26001×10^{-8}

We also calculated values of Jarkslog invariant J_{CP} for these five cases, and found that they lie within present experimental limits (shown in Table 13. Variation of J_{CP} with θ_{13}, taking range of θ_{13} within its 3σ values of its best fit values was also considered (Fig. 4), and find that J_{CP} lies within its experimental limits for these five cases even when variation of θ_{13} is taken. It may be noted that out of the five cases found favourable in our work here, one of the values $\delta_{CP} = 1.43\pi$ matches with the latest global fit value, $\delta_{CP} = 1.4\ \pi$. Future experiments like DUNE/LBNEs and Hyper-Kamionande [38] that would measure δ_{CP} (especially probing leptonic CPV) will support/disfavour the results presented in this work.

TABLE 13

PREFERRED CASES OF CPV, OCTANT, HIERARCHY AND J_{CP} ALLOWED BY PRESENT RANGE, $5.7\times10^{-10} < H_B < 6.7\times10^{-10}$

Serial No.	δ_{CP}, hierarchy, octant, J_{CP} of our calculation	Quadrant Of δ_{CP}
1.	$\delta_{CP} = 1.43\pi$, IH, HO, $J_{CP} = -.03439461$	third quadrant
2.	$\delta_{CP} = 1.727\pi$, IH, LO, $J_{CP} = -.026588173$	fourth quadrant
3.	$\delta_{CP} = 0.5277\pi$, IH, HO, $J_{CP} = .035095635$	second quadrant
4.	$\delta_{CP} = 0.488\pi$, IH, LO, $J_{CP} = .035208214$	first quadarnt
5.	$\delta_{CP} = 0.383\pi$, IH, HO, $J_{CP} = .032889754$	first quadrant

ACKNOWLEDGMENT

GG would like to thank UGC, India, for providing RFSMS fellowship to her, during which part of this work was done. DD thanks HRI, Allahabad, India for providing a postdoctoral fellowship to him. KB thanks DST-SERB, Govt of India, for financial support through a project.

REFERENCES

[1] G. FOGLI, E. LISI, A. MARRONE, D. MONTANINO, A. PALAZZO, ET AL., PHYS. REV. D86, 013012 (2012). ARXIV:1205.5254 [HEP-PH]

[2] D. FORERO, M. TORTOLA, AND J. VALLE, PHYS REV. D86, 073012 (2012). ARXIV:1205.4018 [HEP-PH]

[3] M. GONZALEZ-GARCIA, M. MALTONI, J. SALVADO, AND T. SCHWETZ, JHEP 1212, 123 (2012). ARXIV:1209.3023 [HEP-PH]

[4] DEBAJYOTI DUTTA, KALPANA BORA, MOD. PHYS. LETT. A30(07), 1550017, (2015). ARXIV:1409.8248

[5] MONOJIT GHOSH, POMITA GHOSHAL, SRUBABATI GOSWAMI, SUSHANT K. RAUT, NUCL. PHYS. B884, 274-304 (2014).

ARXIV:1401.7243

[6] I. GIRARDI, S. T. PETCOV, A.V. TITOV, EUR. PHYS. J. C75(7), 345 (2015). ARXIV:1504.00658.

[7] SIN KYU KANG, M TANIMOTO, PHYS. REV. D91(7), 073010 (2015). ARXIV:1411.3104.

[8] LHCB COLLABORATION (ROEL AAIJ (NIKHEF, AMSTERDAM) ET AL.) PHYS. REV. LETT. 114, 041801, 4 (2015), ARXIV:1504.00658.

LHCB-PAPER-2014-059, CERN-PH-EP-2014-271, LHCB-PAPER-2014-059-AND-CERN-PH-EP-2014-271

[9] PATRICK HUBER, MANFRED LINDNER, THOMAS SCHWETZ, WALTER WINTER, JHEP 0911 044 (2009). ARXIV:0907.1896

[10] KALPANA BORA, DEBAJYOTI DUTTA, POMITA GHOSHAL, MOD. PHYS. LETT. A30(14), 1550066, (2015). ARXIV:1405.7482

[11] M. C. GONZALEZ-GARCIA, M. MALTONI, A. YU. SMIRNOV, PHYS. REV. D70, 093005 (2004). HEP-PH/0408170

[12] ANIMESH CHATTERJEE, POMITA GHOSHAL, SRUBABATI GOSWAMI, SUSHANT K.RAUT, JHEP 1306, 010(2013). ARXIV:1302.1370

[13] SANDHYA CHOUBEY, ANUSHREE GHOSH, JHEP 1311, 166 (2013). ARXIV:1309.5760

[14] DALJEET KAUR, NAIMUDDIN, SANJEEV KUMAR, EUR. PHYS. J. C75(4), 156(2014). ARXIV:1302.1370

[15] LBNE COLLABORATION, C. ADAMS ET AL., ARXIV:1307.7335.

[16] T. AKIRI ET AL. [LBNE COLLABORATION], ARXIV:1110.6249 [HEP- EX]

[17] NONA COLLABORATION, D. AYRES ET AL., HEP-EX/0503053.

[18] T2K COLLABORATION, K. ABE ET AL., PHYS. REV. LETT. 107, 041801 (2011). ARXIV:1106.2822

[19] MINOS COLLABORATION, P. ADAMSON ET AL., PHYS. REV. LETT. 107 181802 (2011). ARXIV:1108.0015

[20] D. AUTIERO, J. AYSTO, A. BADERTSCHER, L. B. BEZRUKOV, J. BOUCHEZ, ET AL., JCAP 0711, 011 (2007). ARXIV:0705.0116

[21] G. C. BRANCO, R. G. FELIPE AND F. R. JOAQUIM, REV. MOD. PHYS. 84, 515 (2012). ARXIV:1111.5332 [HEP-PH].

[22] F. P. AN ET AL. [DAYA BAY COLLABORATION], PHYS. REV. LETT, 108, 171803 (2012); CHIN. PHYS.C 37, 011001 (2013),

ARXIV:1210.6327 [HEP-EX]; J. K. AHN ET AL. [RENO COLLABORATION], PHYS. REV. LETT. 108, 191802 (2012). ARXIV:1204.0626

[HEP-EX]; Y. ABE ET AL. [DOUBLE CHOOZ COLLABORATION] PHYS. REV. LETT., 108, 131801 (2012).

[23] B. PONTECORVO. SOV. PHYS. JETP, 6, 429, 1957 ; SOV. PHYS. JETP, 26, 984, (1968) ; Z. MAKI, M. NAKAGAWA AND S. SAKATA,

PROG. THEOR. PHYS., 28, 870 (1962).

[24] F. CAPOZZI, G.L. FOGLI, E. LISI, A. MARRONE, D. MONTANINO, A. PALAZZO , PHYS. REV. D89, 093018 (2014), ARXIV:1312.2878

[HEP-PH]; G. L. FOGLI, E. LISI, A. MARRONE, D. MONTANINO, A. PALAZZO AND A. M. ROTUNNO, PHYS. REV. D 86, 013012 (2012),

ARXIV:1205.5254 [HEP-PH]; D. V. FORERO, M. TORTOLA AND J. W. F. VALLE, PHYS. REV. D 90 (2014), ARXIV:1405.7540 [HEP-PH].

[25] M. C. GONZALEZ-GARCIA, M. MALTONI AND T. SCHWETZ, JHEP 1411, 052 (2014), ARXIV:1409.5439 [HEP-PH].

[26] V. BARGER, D. MARFATIA, AND K. WHISNANT, PHYS. REV. D66, 053007 HEP-PH/0206038.

[27] H. MINAKATA AND H. NUNOKAWA, JHEP 0110, 001 (2001). HEP-PH/0108085

[28] K. A. OLIVE ET AL. [PARTICLE DATA GROUP COLLABORATION], CHIN. PHYS. C 38, 090001 (2014); D. V. FORERO, M. TORTOLA AND J.W. F. VALLE, NEUTRINO OSCILLATIONS REFITTED, PHYS. REV. D 90 (2014) 093006, [1405.7540]; G.L. FOGLI, E. LISI, A. MARRONE,D. MONTANINO, A. PALAZZO, AND A.M. ROTUNNO, PHYS. REV. D 86, 013012 (2012); M.C. GONZALEZ-GARCIA, M. MALTONI, J.SALVADO, AND T. SCHWETZ, JHEP 1212, 123 (2012); F. CAPOZZI, G. L. FOGLI, E. LISI, A. MARRONE, D. MONTANINO AND A.PALAZZO, ARXIV:1312.2878 [HEP-PH].

[29] KALPANA BORA, GAYATRI GHOSH (GAUHATI U.), DEBAJYOTI DUTTA (HARISH-CHANDRA RES. INST.). ADV.HIGH ENERGY PHYS. 2016 (2016) 9496758 , W. BUCHMULLER, P. DI BARI (DESY), M. PLUMACHER, NUCL.PHYS. B643, 367-390 (2002), NUCL.PHYS. B793, 362 (2008), HEP-PH/0205349.

[30] R.N. MOHAPATRA, HAI-BO YU, PHYS.LETT. B644, 346-351 (2007), HEP-PH/0610023

[31] S. BHUPAL DEV. TALK PRESENTED AT DAE HEP SYMPOSIUM, IITG, DEC 8-12, 2014.

[32] P.S. BHUPAL DEV, CHANG-HUN LEE, R.N. MOHAPATRA, J. PHYS. CONF. SER. 6311, 012007 (2015)

[33] GAYATRI GHOSH, KALPANA BORA, TALK PRESENTED AT DAE HEP SYMPOSIUM, IITG, DEC 8-12, 2014, SPRINGER PROC. PHYS. 174

(2016) 287-291.

[34] Z. MAKI, M. NAKAGAWA AND S. SAKATA, PROG. THEOR. PHYS. 28, 870 (1962).

[35] NARENDRA SAHU, S.UMA SANKAR, PHYS.REV. D71, 013006 (2005), HEP-PH/0406065

[36] B. D. FIELDS, P. MOLARTO AND S. SARKAR, "BIG BANG NUCLEOSYNTHESIS," IN REVIEW OF PDG-2014 (ASTROPHYSICAL CONSTANTS AND PARAMETERS)

[37] S. DAVIDSON AND A. IBARRA, PHYS. LETT. B 535, 25 (2002). ARXIV: HEP-PH/0202239.

[38] MATTHEW MALEK, TALK PRESENTED AT 17TH LOMONOSCOV CONFERENCE ON ELEMENTARY PARTICLE PHYSICS, MOSCOW STATE UNIVERSITY